

# Analysis of 2D Thin Walled Structures in BEM with High-Order Geometry Elements Using Exact Integration

Yaoming Zhang<sup>1</sup>, Yan Gu<sup>1</sup> and Jeng-Tzong Chen<sup>2</sup>

**Abstract:** There exist nearly singular integrals for thin walled structures in the boundary element method (BEM). In this paper, an efficient analytical method is developed to deal with the nearly singular integrals in the boundary integral equations (BIEs) for 2-D thin walled structures. The developed method is possible for problems defined in high-order geometry elements when the nearly singular integrals need to be calculated. For the analysis of nearly singular integrals with high-order geometry elements, much fewer boundary elements can be used to achieve higher accuracy. More importantly, computational models of thin walled structures or thin shapes in structures demand a higher level of the geometry approximation to the original domains, and the usage of high-order geometry in computational models can meet this requirement. Three numerical examples are presented to test the developed method and very promising results are obtained when the thickness-to-length ratio is in the orders of 1E-01 to 1E-06, which is sufficient for modeling most thin structures in industrial applications.

**Keywords:** BEM, elasticity problem, curved boundary, nearly singular integrals, thin walled structures, exact integrations.

## 1 Introduction

Thin-body structures are frequently used for the design in various industrial applications, including solid mechanics, acoustics and electromagnetism [Chen and Liu (2001); Albuquerque and Aliabadi (2008);Guz *et al.* (2007); Karlis *et al.* (2008)]. Numerical analysis of the behavior of these structures represents a great challenge to researchers in computational mechanics. Studies show that the conventional boundary element method (CBEM) using the standard Gaussian quadrature fails to

---

<sup>1</sup> Institute of Applied Mathematics, Shandong University of Technology, Zibo 255049, P.R. China, E-mail: zymfc@163.com

<sup>2</sup> Department of Harbor and River Engineering, National Taiwan Ocean University, Keelung 20224, Taiwan, E-mail: jtchen@mail.ntou.edu.tw

yield reliable results for these structures. The major reason for this failure is that the kernels' integration presents various orders of near singularities, owing to the mesh on one side of the thin-body being too close to the mesh on the opposite side. Moreover, the nearly singular problem may also occur when the interior physical quantity need to be calculated.

Nearly singular integrals are not singular in the sense of mathematics. However, from the point of view of numerical integrations, these integrals can not be calculated accurately by using the conventional numerical quadrature since the integrand oscillates very fiercely within the integration interval. Other than the nearly singular integral, many direct and indirect algorithms for singular integral have been developed and used successfully [Atluri (2004, 2005);Atluri *et al.* (2003, 2006);Okada *et al.* (1990);Han *et al.* (2003, 2007);Brebbia *et al.* (1984);Chen (2002, 2000);Davies *et al.*(2007);Li, Wu and Yu (2009);Sanz *et al.* (2007);Sun (1999);Tanaka, Sladek (1994); Guiggiani (1992);Young *et al.* (2007);Zhang *et al.* (2004)]. Therefore, the key point in achieving the required accuracy and efficiency of the BEM is not the singular integral but the nearly singular integral. Although that difficulty can be overcome by using very fine meshes, the process requires too much preprocessing and CPU time.

Owing to the importance of the nearly singular integrals, many numerical methods and techniques have been developed in the past decades. These proposed methods can be divided on the whole into two categories: "indirect algorithms" and "direct algorithms". The indirect algorithms [Okada *et al.* (1989, 1990); Sladek *et al.* (1993);Zhang and Sun (2000);Liu *et al.* (2008);Mukerjee (2000)], which benefit from the regularization ideas and techniques for the singular integrals, are mainly to calculate indirectly or avoid calculating the nearly singular integrals by establishing new regularized boundary integral equations (BIEs). The direct algorithms are calculating the nearly singular integrals directly. They usually include interval subdivision method [Jun (1985);Tanaka (1991)], special Gaussian quadrature method [Earlin (1992);Lifeng (2004)], and various nonlinear transformation method [Luo *et al.* (1998);Liu *et al.* (2000,2008) Zhang and Sun (2008)].

Analytical integration is an alternative way to improve the calculation accuracy of the nearly singular integrals. Various analytical schemes have been developed over the past years. Yoon *et al.* (2000) proposed an exact expression of kernel integrals with the linear isoparametric element; Fratantonio and Rencis (2000) derived exact integrations for the constant, linear and quadratic elements, while the geometrical boundaries were all depicted by using linear shape functions; Zhang and Sun (2001) established an analytical scheme, which is both available for singular and nearly singular integrals, to treat the boundary integrals of two-dimensional potential and elastic problems. Zhang *et al.* (2004) derived the exact integrations

for 2-D elastostatic problems, in which the boundary quantities are approximated by using various order discontinuous interpolation functions and the boundary geometry is also depicted by using straight line; Niu *et al.* (2007) and Zhou *et al.* (2008) proposed the semi-analytical or analytical integral formulas to calculate the nearly singular integrals for both potential and elastic problems, and suggested a strategy to deal with the isoparametric quadratic elements. The strategy replace the parabolic arcs with two or more straight line segments; By means of the symbolic computer program Mathematica, Padhi *et al.* (2001) derived an analytic formulation of the nearly singular integrals in the displacement BIE of 2-D elasticity with the Taylor's series approximation to  $\ln r$ ,  $1/r$  and the Jacobian.

For most of the current numerical methods, especially for the exact integration method, the geometry of the boundary element is often depicted by using linear shape functions when nearly singular integrals need to be calculated. However, most engineering processes occur mostly in complex geometrical domains, and obviously, higher order geometry elements are expected to be more accurate to solve such practical problems [Atluri (2005)]. Therefore, to improve the calculation accuracy and efficiency of the nearly singular integrals, efficient approaches are available for high order geometry elements are necessary and need to be further investigated.

Recently, a general transformation method suitable for calculating the nearly singular integrals occurring on high order geometry elements was proposed by authors of this paper [Zhang, Gu and Chen (2009)]. Although thin-body problems are not considered on their research, this transformation has potential to effectively treat this kind of problems.

When the geometry of the boundary element is approximated by using high-order elements—usually of second order, the Jacobian  $J(\xi)$  is not a constant but a non-rational function which can be expressed as  $\sqrt{a + b\xi + c\xi^2}$ , where  $a$ ,  $b$  and  $c$  are constants,  $\xi$  is the dimensionless coordinate; The distance  $r$  between the field points and the source point is a non-rational function of the type  $\sqrt{p_4(\xi)}$ , where  $p_4(\xi)$  is the fourth order polynomial. Thus, the forms of the integrands in boundary integrals become more complex, and for a long time, it was even thought that the implementation of the exact integration is impossible in this situation.

It is well known that the domain variables can be computed by integral equations after all the boundary quantities have been obtained, and the accuracy of boundary quantities directly affects the validity of the interior quantities. Therefore, for dealing with thin-body problems, two aspects are necessary: one is the accurate computation of the boundary unknown quantities, which is generally carried out by adopting the regularized boundary integral equations (BIEs) for the calculation of singular integrals; the other is an efficient algorithm for calculating the nearly sin-

gular integrals. In addition, for thin-body problems, some boundary elements will be very close to each other. Thus, the singular and nearly singular integrals need to be evaluated simultaneously when calculating the boundary unknown variables.

In this paper, a new exact integration method for estimating nearly singular integrals occurring on curvilinear geometries is presented. The proposed strategy bases on a kind of inverse interpolation technique and uses a series of interpolation polynomials to approximate the regular part of the integrand such as the Jacobian, the shape functions and a finite sum of polynomials divided by  $r^n$ . Therefore, the original complicated integrands can be substituted by some simple polynomials, and then the whole integral can be calculated straightforwardly by using analytical integral formulations. The exact integrations derived in this paper substantially simplify the programming and provided a general computational method for evaluating the nearly singular integrals. This paper applies the new analytical formulas to deal with the nearly singular integrals for 2-D elasticity problems of thin bodies, and very promising results are obtained when the thickness to length ratio is in the orders from 1.0E-1 to 1.0E-6, which is sufficient for modeling most thin structures in industrial applications.

Moreover, it will be seen that the exact integration method proposed in this paper also provide an effective scheme for calculating those complex integrals which have been thought to be impossible to find an exact representation.

## 2 Non-singular boundary integral equations (BIEs)

In this paper, we always assume that  $\Omega$  is a bounded domain in  $R^2$ ,  $\Omega^c$  is its open complement, and  $\Gamma$  denotes the boundary.  $\mathbf{t}(\mathbf{x})$  and  $\mathbf{n}(\mathbf{x})$  (or  $\mathbf{t}$  and  $\mathbf{n}$ ) are the unit tangent and outward normal vectors of  $\Gamma$  to the domain  $\Omega$  at the point  $\mathbf{x}$ , respectively. For 2-D elastic problems, the non-singular BIEs with indirect variables are given in [Zhang *et al.* (2004)]. Without regard to the rigid body displacement and the body forces, the non-singular BIEs on  $\Omega^c$  can be expressed as

$$u_i(\mathbf{y}) = \int_{\Gamma} \varphi_k(\mathbf{x}) u_{ik}^*(\mathbf{y}, \mathbf{x}) d\Gamma, \mathbf{y} \in \Gamma \quad (1)$$

$$\begin{aligned} \nabla u_i(\mathbf{y}) = & \int_{\Gamma} [\varphi_k(\mathbf{x}) - \varphi_k(\mathbf{y})] \nabla u_{ik}^*(\mathbf{y}, \mathbf{x}) d\Gamma - \varphi_k(\mathbf{y}) \left\{ \int_{\Gamma} [\mathbf{t}(\mathbf{x}) - \mathbf{t}(\mathbf{y})] \frac{\partial u_{ik}^*(\mathbf{y}, \mathbf{x})}{\partial \mathbf{t}} d\Gamma \right. \\ & + \int_{\Gamma} [\mathbf{n}(\mathbf{x}) - \mathbf{n}(\mathbf{y})] \frac{\partial u_{ik}^*(\mathbf{y}, \mathbf{x})}{\partial \mathbf{n}} d\Gamma + \frac{k_0}{G} \mathbf{n}(\mathbf{y}) \left( \int_{\Gamma} [n_k(\mathbf{x}) - n_k(\mathbf{y})] \frac{\partial \ln r}{\partial x_i} d\Gamma \right. \\ & \left. \left. + n_k(\mathbf{y}) \int_{\Gamma} [t_i(\mathbf{x}) - t_i(\mathbf{y})] \frac{\partial \ln r}{\partial \mathbf{t}} d\Gamma + n_k(\mathbf{y}) \int_{\Gamma} [n_i(\mathbf{x}) - n_i(\mathbf{y})] \frac{\partial \ln r}{\partial \mathbf{n}} d\Gamma \right) \right\}, \mathbf{y} \in \Gamma \quad (2) \end{aligned}$$

For the domain  $\Omega$ , the nonsingular BIEs are given as

$$u_i(\mathbf{y}) = \int_{\Gamma} \phi_k(\mathbf{x}) u_{ik}^*(\mathbf{x}, \mathbf{y}) d\Gamma, \quad \mathbf{y} \in \Gamma \quad (3)$$

$$\begin{aligned} \nabla u_i(\mathbf{y}) = & \phi_k(\mathbf{y}) \mathbf{n}(\mathbf{y}) \frac{1}{G} \left[ \delta_{ik} - \frac{n_k(\mathbf{y}) n_i(\mathbf{y})}{2(1-\nu)} \right] + \int_{\Gamma} [\phi_k(\mathbf{x}) - \phi_k(\mathbf{y})] \nabla u_{ik}^*(\mathbf{y}, \mathbf{x}) d\Gamma \\ & - \phi_k(\mathbf{y}) \left\{ \int_{\Gamma} [\mathbf{t}(\mathbf{x}) - \mathbf{t}(\mathbf{y})] \frac{\partial u_{ik}^*(\mathbf{y}, \mathbf{x})}{\partial \mathbf{t}} d\Gamma + \int_{\Gamma} [\mathbf{n}(\mathbf{x}) - \mathbf{n}(\mathbf{y})] \frac{\partial u_{ik}^*(\mathbf{y}, \mathbf{x})}{\partial \mathbf{n}} d\Gamma \right. \\ & + \frac{k_0}{G} \mathbf{n}(\mathbf{y}) \left( \int_{\Gamma} [n_k(\mathbf{x}) - n_k(\mathbf{y})] \frac{\partial \ln r}{\partial x_i} d\Gamma + n_k(\mathbf{y}) \int_{\Gamma} [t_i(\mathbf{x}) - t_i(\mathbf{y})] \frac{\partial \ln r}{\partial \mathbf{t}} d\Gamma \right. \\ & \left. \left. + n_k(\mathbf{y}) \int_{\Gamma} [n_i(\mathbf{x}) - n_i(\mathbf{y})] \frac{\partial \ln r}{\partial \mathbf{n}} d\Gamma \right) \right\}, \quad \mathbf{y} \in \Gamma \quad (4) \end{aligned}$$

For the internal point  $\mathbf{y}$ , the integral equations can be written as

$$u_i(\mathbf{y}) = \int_{\Gamma} \phi_k(\mathbf{x}) u_{ik}^*(\mathbf{y}, \mathbf{x}) d\Gamma, \quad \mathbf{y} \in \hat{\Omega} \quad (5)$$

$$\nabla u_i(\mathbf{y}) = \int_{\Gamma} \phi_k(\mathbf{x}) \nabla u_{ik}^*(\mathbf{y}, \mathbf{x}) d\Gamma, \quad \mathbf{y} \in \hat{\Omega} \quad (6)$$

In Eqs. (1)~(6),  $i, k = 1, 2$ ;  $k_0 = 1/4\pi(1-\nu)$ ;  $G$  is the shear modulus;  $\phi_k(\mathbf{x})$  is the density function to be determined;  $u_{ik}^*(\mathbf{y}, \mathbf{x})$  denotes the Kelvin fundamental solution. In Eqs. (5) and (6)  $\hat{\Omega} = \Omega$  or  $\Omega^c$ .

The Gaussian quadrature is directly used to calculate the integrals in discretized equations in the conventional boundary element method. However, if the domain of a considered problem is thin, some boundaries will be very close to each other. Thus, the distance  $r$  between some boundary nodes and boundary integral elements probably approaches zero. This causes the integrals in discretized Eqs. (1)~(4) nearly singular, and the results of the Gaussian quadrature become invalid. Therefore, the density functions cannot be calculated accurately, needless to say, to calculate the physical quantities at interior points. Moreover, almost all the interior points of thin bodies are very close to the integral elements. Thus, there also exist nearly singular integrals in Eqs. (5) and (6). These nearly singular integrals can be expressed as

$$\begin{cases} I_1 = \int_{\Gamma_e} \psi(\mathbf{x}) \ln r^2 d\Gamma \\ I_2 = \int_{\Gamma_e} \psi(\mathbf{x}) \frac{1}{r^{2\alpha}} d\Gamma \end{cases} \quad (7)$$

where  $\alpha > 0$ ,  $\psi(\mathbf{x})$  denotes a well-behaved function.

### 3 Nearly singular integrals over curvilinear elements

The quintessence of the BEM is to discretize the boundary into a finite number of segments, not necessarily equal, which are called boundary elements. Two approximations are made over each of these elements. One is about the geometry of the boundary, while the other has to do with the variation of the unknown boundary quantity over the element. The linear element is not an ideal one as it can not approximate with sufficient accuracy for the geometry of curvilinear boundaries. For this reason, it is recommended to use higher order elements, namely, elements that approximate geometry and boundary quantities by higher order interpolation polynomials—usually of second order. In this paper, the geometry segment is modeled by a continuous parabolic element, which has three knots, two of which are placed at the extreme ends and the third somewhere in-between, usually at the midpoint. Therefore the boundary geometry is approximated by a continuous piecewise parabolic curve. On the other hand, the distribution of the boundary quantity on each of these elements is depicted by a discontinuous quadratic element, three nodes of which are located away from the endpoints.

Assume  $\mathbf{x}^1 = (x_1^1, x_2^1)$  and  $\mathbf{x}^2 = (x_1^2, x_2^2)$  are the two extreme points of the segment  $\Gamma_j$ , and  $\mathbf{x}^3 = (x_1^3, x_2^3)$  is in-between one. Then the element  $\Gamma_j$  can be expressed as follows

$$x_k(\xi) = N_1(\xi)x_k^1 + N_2(\xi)x_k^2 + N_3(\xi)x_k^3, k = 1, 2$$

where  $N_1(\xi) = \xi(\xi - 1)/2$ ,  $N_2(\xi) = \xi(\xi + 1)/2$ ,  $N_3(\xi) = (1 - \xi)(1 + \xi)$ ,  $-1 \leq \xi \leq 1$ .

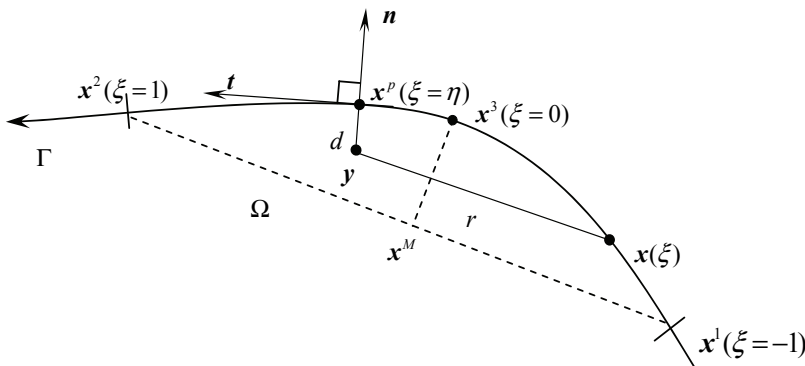


Figure 1: The minimum distance  $d$  from the field point  $y$  to the boundary element

As shown in Fig. 1, the minimum distance  $d$  from the field point  $\mathbf{y} = (y_1, y_2)$  to the boundary element  $\Gamma_j$  is defined as the length of  $\overline{\mathbf{y}\mathbf{x}^p}$ , which is perpendicular to the tangential line  $\mathbf{t}$  and through the projection point  $\mathbf{x}^p$ . Letting  $\eta \in (-1, 1)$  is the local coordinate of the projection point  $\mathbf{x}^p$ , i.e.  $\mathbf{x}^p = (x_1(\eta), x_2(\eta))$ . Then  $\eta$  is the real root of the following equation

$$x'_k(\eta)(x_k(\eta) - y_k) = 0 \quad (8)$$

If the field point  $\mathbf{y}$  sufficiently approaches the boundary, then Eq. (8) has a unique real root. In fact, setting

$$F(\eta) = x'_k(\eta)(x_k(\eta) - y_k)$$

$$F'(\eta) = x'_k(\eta)x'_k(\eta) + x''_k(\eta)(x_k(\eta) - y_k) = J^2(\eta) + x''_k(\eta)(x_k(\eta) - y_k)$$

where  $J(\eta)$  is the Jacobian of the transformation from parabolic element to the line interval  $[-1, 1]$ . Therefore, when the field point  $\mathbf{y}$  is sufficiently close to the element, we explicitly have  $F'(\eta) > 0$ .

The unique real root of Eq. (8) can be evaluated numerically by using the Newton's method or computed exactly by adopting the algebraic root formulas of 3-th algebraic equations. In this paper, two ways are all tested, and practical applications show that both ways can be used to obtain desired results. Furthermore, the Newton's method is more simple and effective, especially if the initial approximation is properly chosen and if we can do this, only two or three iterations are sufficient to approximate the real root. For the root formula of 3-th algebraic equations, let's consider the following algebraic equation

$$ax^3 + bx^2 + cx + d = 0$$

if there exists only one real root, the analytical solution can be expressed as follows

$$x = -\frac{b}{3a} + \frac{2(\sqrt{s^2 + t^2})^{\frac{1}{3}}}{3\sqrt[3]{2a}} \cos\left(\frac{1}{3} \arccos \frac{s}{\sqrt{s^2 + t^2}}\right)$$

where  $s = -2b^3 + 9acb - 27a^2d$ ,  $t = \sqrt{-4(3ac - b^2)^3 - (-2b^3 + 9acb - 27a^2d)^2}$ .

Using the procedures described above, we can obtain the value of the real root  $\eta$ . Thus, we have

$$\begin{aligned} x_k - y_k &= x_k - x_k^p + x_k^p - y_k \\ &= \frac{1}{2}(\xi - \eta) [(x_k^1 - 2x_k^3 + x_k^2)(\xi + \eta) + (x_k^2 - x_k^1)] + x_k(\eta) - y_k \end{aligned} \quad (9)$$

By using Eq. (9), the distance square  $r^2$  between the field point  $\mathbf{y}$  and the source point  $\mathbf{x}(\xi)$  can be written as

$$r^2(\xi) = (x_k - y_k)(x_k - y_k) = (\xi - \eta)^2 g(\xi) + d^2 \quad (10)$$

where  $d^2 = (x_k(\eta) - y_k)(x_k(\eta) - y_k)$ ,

$$g(\xi) = \frac{1}{4}(x_k^1 - 2x_k^3 + x_k^2)(x_k^1 - 2x_k^3 + x_k^2)(\xi + \eta)^2 + \frac{1}{2}(x_k^1 - 2x_k^3 + x_k^2)(x_k^2 - x_k^1)(\xi + \eta) + h^2 + (x_k^1 - 2x_k^3 + x_k^2)(x_k(\eta) - y_k), \text{ where } h = \frac{1}{2}\sqrt{(x_k^2 - x_k^1)(x_k^2 - x_k^1)}.$$

Apparently, there is  $g(\xi) \geq 0$ . Furthermore, under some assumptions we can also prove that  $g(\xi) > 0$ . As shown in Fig. 1,  $\mathbf{x}^M$  is the midpoint of the line  $\overline{\mathbf{x}^1\mathbf{x}^2}$ . For simplicity, we take  $\mathbf{x}^3$  to satisfy that  $\overline{\mathbf{x}^M\mathbf{x}^3}$  is perpendicular to  $\overline{\mathbf{x}^1\mathbf{x}^2}$ , i.e.  $(x_k^1 - 2x_k^3 + x_k^2)(x_k^2 - x_k^1) = 0$ . So

$$g(\xi) \geq h^2 + (x_k^1 - 2x_k^3 + x_k^2)(x_k(\eta) - y_k)$$

Therefore, if the minimum distance  $d$  is sufficiently small, it follows that  $g(\xi) > 0$ .

#### 4 Exact integrations for nearly singular integrals

With the aid of the Eq. (10), the nearly singular integrals in Eq. (7) can be rewritten as

$$\begin{cases} I_1 = \int_{-1}^1 |J| f(\xi) \ln((\xi - \eta)^2 g(\xi) + d^2) d\xi \\ I_2 = \int_{-1}^1 \frac{|J| f(\xi)}{((\xi - \eta)^2 g(\xi) + d^2)^\alpha} d\xi \end{cases} \quad (11)$$

where  $|J| = \sqrt{(\frac{dx_1}{d\xi})^2 + (\frac{dx_2}{d\xi})^2}$  represents the Jacobian;  $f(\cdot)$  is a regular function that consists of shape functions, and ones which arise from taking the derivative of the integral kernels.

Introduce the following coordinate transformation

$$t = \Phi(\xi) = (\xi - \eta)\sqrt{g(\xi)} \quad (12)$$

We can easily prove that  $\Phi'(\xi) \neq 0$ . In fact

$$\Phi'(\xi) = \frac{2g(\xi) + (\xi - \eta)g'(\xi)}{2\sqrt{g(\xi)}}, \quad r' = \frac{(\xi - \eta)[2g(\xi) + (\xi - \eta)g'(\xi)]}{2\sqrt{(\xi - \eta)^2 g(\xi) + d^2}}$$

$\Phi'(\xi) \neq 0$  is equivalent to the fact that the equation  $r'(\xi) = 0$  has only one root  $\xi = \eta$  within the interval  $[-1, 1]$ . Actually, if the field point  $\mathbf{y}$  sufficiently approaches the boundary element, the assertion must hold.

Substituting (12) into (11), we obtain the following equations

$$\begin{cases} I_1 &= \int_{t_1}^{t_2} \frac{|J|f(\xi)}{\Phi'(\xi)} \ln(t^2 + d^2) dt = \int_{t_1}^{t_2} F(\xi) \ln(t^2 + d^2) dt \\ I_2 &= \int_{t_1}^{t_2} \frac{|J|f(\xi)}{\Phi'(\xi)} \frac{1}{(t^2 + d^2)^\alpha} dt = \int_{t_1}^{t_2} F(\xi) \frac{1}{(t^2 + d^2)^\alpha} dt \end{cases} \quad (13)$$

where  $t_1 = -(1 + \eta)\sqrt{g(-1)}$ ,  $t_2 = (1 - \eta)\sqrt{g(1)}$ ,  $F(\xi) = |J|f(\xi)/\Phi'(\xi)$ .

Generally, it is impossible to obtain the exact expression of  $\xi$  from  $t = \Phi(\xi)$ . In other words,  $F(\xi)$  can not be easily expressed with respect to the variable  $t$ . In order to find an approximate expression of  $F(\xi)$ , we adopt a kind of inverse interpolation idea and technique, using a series of interpolation polynomials to approximate the regular part  $F(\xi)$ . In order to make this point clear, we select seven interpolation nodes, as shown in Fig. 2, since a sextic interpolation polynomial has been found satisfactory in practice.

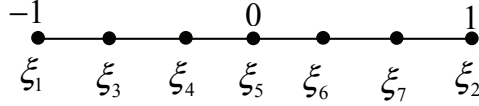


Figure 2: inverse interpolation nodes

Then the sextic interpolation function for  $F(\xi)$  can be written as

$$F(\xi) \approx \sum_{i=1}^7 \prod_{\substack{j=1 \\ j \neq i}}^7 \frac{(t - t_j)}{(t_i - t_j)} F(\xi_i)$$

where  $t_i = (\xi_i - \eta)\sqrt{g(\xi_i)}$ ,  $i = 1 \sim 7$ .

Using the procedure described above, Eq. (13) can be expressed as a series of elementary integrals, as shown in (14), which can now be calculated exactly by using completely analytical integral formulas.

$$I_1 = \int_{t_1}^{t_2} t^i \ln(t^2 + d^2) dt, \quad I_2 = \int_{t_1}^{t_2} \frac{t^i}{(t^2 + d^2)^\alpha} dt, \quad i = 1, \dots, 6 \quad (14)$$

## 5 Numerical examples

To begin with, an example of boundary layer effect is considered to testify the feasibility of the proposed method, which the physical quantities at interior point very close to the boundary are calculated. Whereafter, two thin walled structures with various thickness-to-length ratios are considered.

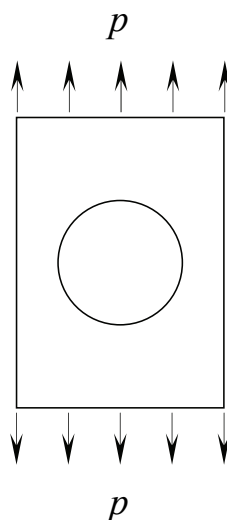


Figure 3: An infinite plate with a circular hole subjected to the uniform tensile forces

**Example 1** This example is given to test the feasibility of the proposed method. As shown in Fig. 3, an infinite plate with a circular hole subjected to the uniform tensile forces  $p = 10$  at infinity is considered. The radius of the circle is  $r = 2$ . In this example, the elastic shear modulus is  $G = 807692.3N/cm^2$ , and the Poisson's ratio is  $\nu = 0.3$ . There are 30 uniform quadratic boundary elements divided along the circular boundary.

The results of the tangential and radial stresses  $\sigma_\theta$ ,  $\sigma_r$  at interior points on the line  $x_2 = 0$  are listed in Tab. 1 and Fig. 4, respectively. The convergence rate of the computed  $\sigma_\theta$  at the point (1E-09, 0) is shown in Fig. 5.

It can be seen from Tab. 1 that the results calculated by the CBEM are not in a good agreement with the analytic solutions as the computed points locate increasingly close to the boundary, i.e., when the distance between the interior point and the boundary is equal to or less than 0.01. However, the results calculated by the proposed method are very consistent with the exact solutions even when the dis-

tance between the interior point and the outer boundary approaches  $1E-10$ . The percentage errors are also listed in Tab. 1, from which we can see that the accuracy of the results calculated by using the present method are satisfactory with the largest relative error less than  $0.02\%$ .

We can observe from Fig. 4 that the results of radial stresses  $\sigma_r$  yields excellent accuracy even when the distance between the interior point and the inner surface reaches  $1E-10$ . In addition, the convergence plot in Fig. 5 shows that the convergence rates of the present method are fast even when the distance between the computed point and the boundary approaches  $1E-09$ .

Table 1: Tangential stresses  $\sigma_\theta$  at interior points on the line  $x_2 = 0$

$x_1$	Exact	CBEM	Present	Relative error (%)
2.1	0.2687568E+02	0.268777E+02	0.2687775E+02	-0.7669777E-02
2.01	0.2965409E+02	0.293976E+02	0.2965912E+02	-0.1696342E-01
2.001	0.2996504E+02	0.305789E+02	0.2997061E+02	-0.1859621E-01
2.0001	0.2999650E+02	0.307377E+02	0.3000213E+02	-0.1876807E-01
2.00001	0.2999965E+02	0.307535E+02	0.3000529E+02	-0.1878534E-01
2.000001	0.2999997E+02	0.307551E+02	0.3000560E+02	-0.1878707E-01
2.0000001	0.3000000E+02	0.307552E+02	0.3000563E+02	-0.1878724E-01
2.00000001	0.3000000E+02	0.307552E+02	0.3000564E+02	-0.1878718E-01
2.000000001	0.3000000E+02	0.307552E+02	0.3000564E+02	-0.1878649E-01
2.0000000001	0.3000000E+02	0.307552E+02	0.3000563E+02	-0.1877948E-01

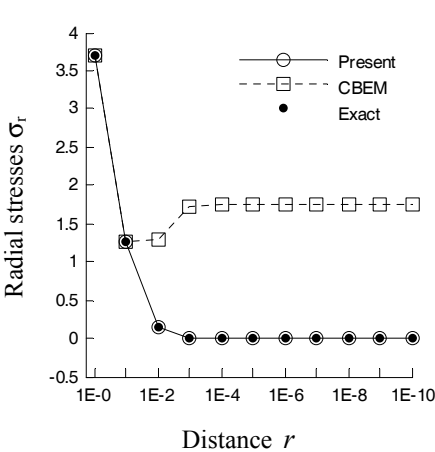


Figure 4: Radial stresses  $\sigma_r$  at interior points on the line  $x_2 = 0$

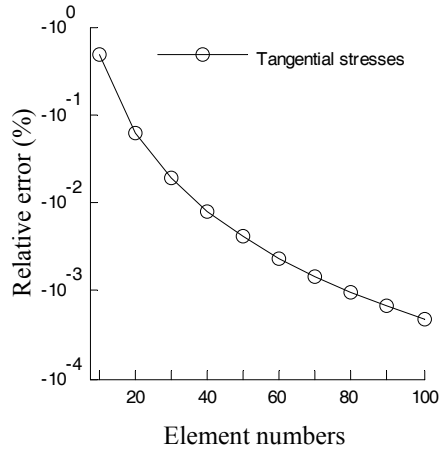


Figure 5: Convergence curve of the computed  $\sigma_\theta$  at the point  $(1E-09, 0)$

**Example 2** As shown in Fig. 6, a thin-walled cylinder subjected to a uniform internal pressure  $p = 1$  is considered. The outer and inner radii of the cylinder are  $a$  and  $b$ , respectively, with  $a = 10$ . The elastic shear modulus is  $G = 807692.3N/cm^2$ , and the Poisson's ratio is  $\nu = 0.3$ .

There are 48 discontinuous isoparametric quadratic elements divided along the outer and inner surfaces. In this example,  $(a - b)/a$  is defined as the thickness-to-length ratio [Zhou et al. (2008)]. As  $a$  is fixed as 10, the ratio reduces as  $b$  decreases.

For different thickness-to-length ratios, the results of the unknown stresses at the boundary node  $A(10, 0)$  are shown in Fig. 7. The results at interior point  $B((a + b)/2, 0)$  are listed in Tab. 2 and Tab. 3. Both the CBEM and the proposed method are employed for the purpose of comparison. For  $(a - b)/a = 1.0E - 6$ , the stresses at interior points on the line  $x_2 = 0$  are listed in Tab. 4; the convergence curves of computed stresses at the interior point  $B$  are shown in Fig. 8.

We can see from Fig. 7 that the calculated results of stresses at the boundary node  $A$  calculated by using the proposed method are very consistent with the exact solutions, with the largest relative error less than 0.5%, even when the thickness-to-length ratio as small as  $1.0E - 6$ .

Tab. 2 and Tab. 3 show that the CBEM can only be available to calculate the acceptable radial and tangential stresses at the interior point  $B$  for the thickness-to-length ratio down to  $1E-01$ , and the results are out of true with further decrease of the thickness-to-length ratio. Nevertheless, the results obtained by using the presented schemes are excellently consistent with the analytical solutions even when the thickness-to-length ratio equals  $1E-06$ .

Tab. 4 presents the results of radial and tangential stresses at eight different interior points on the line  $x_2 = 0$  with the thickness-to-length ratio equals  $1E-06$ , which further demonstrate the effectiveness of the present method.

Table 2: Radial stresses  $\sigma_r$  at the interior point  $B$

$(a - b)/a$	Exact	CBEM	Present	Relative error (%)
2.0E-1	-0.4170096E+00	-0.4168510E+00	-0.4169653E+00	0.1062267E-01
1.0E-1	-0.4605628E+00	-0.4594888E+00	-0.4604442E+00	0.2574519E-01
1.0E-2	-0.4962312E+00	0.3504272E+01	-0.4963201E+00	-0.1790878E-01
1.0E-3	-0.4996248E+00	-0.4890038E+02	-0.4996364E+00	-0.2316737E-02
1.0E-4	-0.4999625E+00	0.4163399E+02	-0.4999636E+00	-0.2268517E-03
1.0E-5	-0.4999962E+00	0.3506209E+02	-0.4999907E+00	0.1117456E-02
1.0E-6	-0.4999996E+00	0.3453840E+02	-0.4993287E+00	0.1341773E+00

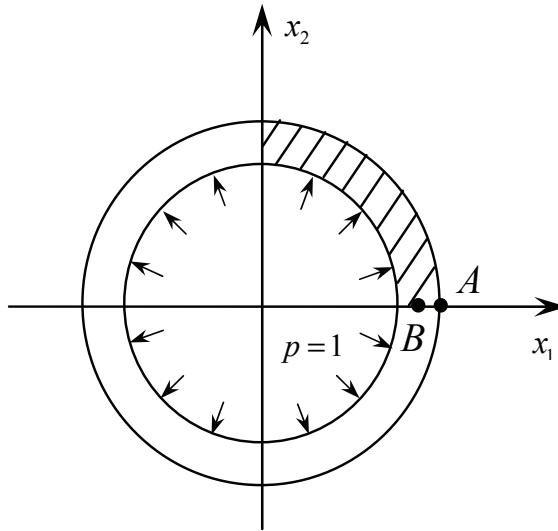


Figure 6: A thin-walled cylinder subjected to uniform internal pressure

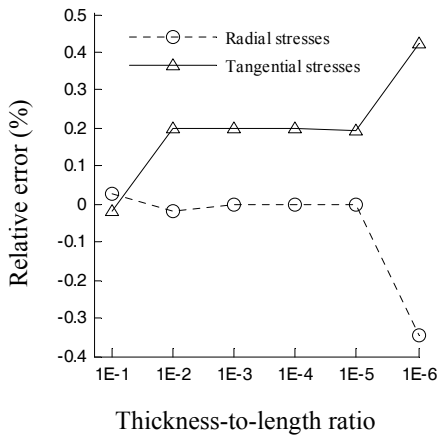


Figure 7: Relative errors of  $\sigma_\theta$  and  $\sigma_r$  at the boundary node A

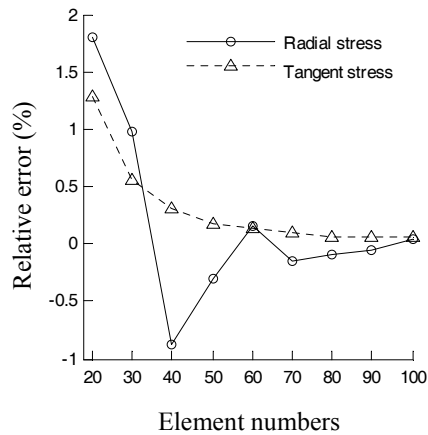


Figure 8: Convergence curves of  $\sigma_\theta$  and  $\sigma_r$  at the interior point B with  $(a - b)/a = 1.0E - 6$

Convergence curves of computed stresses at interior points B by using the presented method are shown in Fig. 8 from which we can observe that the convergence speeds are still fast even when the thickness-to-length ratio reached 1E-06. In Fig. 8, only the errors of the present method are given since the errors of the CBEM are

Table 3: Tangential stresses  $\sigma_\theta$  at the interior point  $B$ 

$(a-b)/a$	Exact	CBEM	Present	Relative error (%)
2.0E-1	0.3972565E+01	0.3972922E+01	0.3972661E+01	-0.2417346E-02
1.0E-1	0.8986879E+01	0.8990797E+01	0.8988732E+01	-0.2062619E-01
1.0E-2	0.9899874E+02	0.1008786E+03	0.9892158E+02	0.7794239E-01
1.0E-3	0.9989999E+03	0.1327530E+04	0.9982280E+03	0.7726567E-01
1.0E-4	0.9999000E+04	-0.1133652E+04	0.9991276E+04	0.7725178E-01
1.0E-5	0.9999900E+05	-0.9566364E+03	0.9992151E+05	0.7749157E-01
1.0E-6	0.9999990E+06	-0.9423957E+03	0.9985437E+06	0.1455262E+00

Table 4: Radial and tangential stresses at interior points on the line  $x_2 = 0$ 

$x_1$	Radial stresses $\sigma_r$		Tangential stresses $\sigma_\theta$	
	Exact	Present	Exact	Present
9.999991	-0.8999999E+00	-0.8975619E+00	0.9999994E+06	0.9985442E+06
9.999992	-0.7999998E+00	-0.7976682E+00	0.9999993E+06	0.9985441E+06
9.999993	-0.6999997E+00	-0.6973147E+00	0.9999992E+06	0.9985440E+06
9.999994	-0.5999996E+00	-0.5979686E+00	0.9999991E+06	0.9985440E+06
9.999996	-0.3999996E+00	-0.4001979E+00	0.9999989E+06	0.9985438E+06
9.999997	-0.2999997E+00	-0.3007079E+00	0.9999988E+06	0.9985437E+06
9.999998	-0.1999998E+00	-0.2007479E+00	0.9999987E+06	0.9985436E+06
9.999999	-0.9999986E-01	-0.1009180E+00	0.9999986E+06	0.9985436E+06

relatively too large.

**Example 3** As shown in Fig. 9, a thin coating with nonuniform thickness on a shaft is considered. Both the shaft and coating profiles remain circular, but their centers are misaligned ( $b$ ) compared to the uniform thickness case ( $a$ ), producing some normalized eccentricity  $\delta = x_c/r_b - r_a$ , where  $x_c$  is the center offset. The coating and shaft have outer radii  $r_a$  and  $r_b$  respectively, with their centre of curvature located at the point  $o(0,0)$ . In this example, the coated system is loaded by a uniform pressure  $p$ , and the shaft is considered to be rigid when compared to the coating, so the boundary conditions are  $u_x = u_y = 0$  for all nodes at the shaft/coating interface. There are totally 16 discontinuous isoparametric quadratic elements divided along the shaft and coating surfaces, regardless of the thickness of the structure. The elastic shear modulus is  $G = 8.0 \times 10^{10}$ Pa, Poisson's ratio is  $\nu = 0.2$ .

While no analytical solution exists for  $\delta \neq 0$  case, the asymptotic behavior of the solution as  $\delta \rightarrow 0$  can be checked to verify the formulation. In this example, shaft radius is held constant at 0.1 and coating outer radius is also constant at 0.11; the eccentricity has been systematically varied over the entire range  $0 \leq \delta < 1$ .

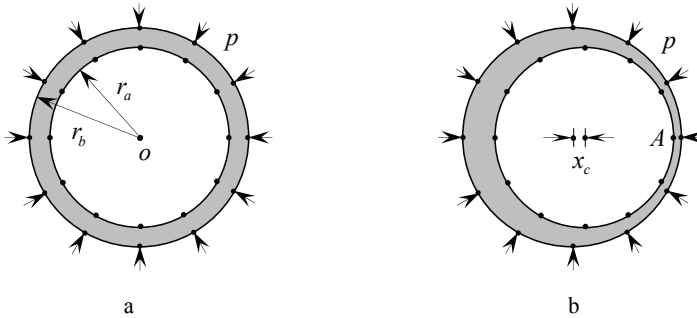


Figure 9: A thin coating with nonuniform thickness on a shaft.

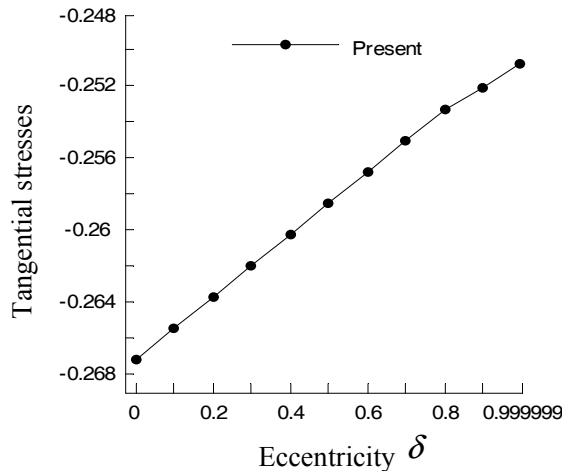


Figure 10: Tangential stress at boundary node A.

In 1998, Luo *et al.* [Luo, Liu and Berger (1998)] have handled this coating system, and the radial stress  $\sigma_r$  at boundary node A has been obtained by using the BEM. However, in their work only boundary unknown radial stresses  $\sigma_r$  are computed. The boundary unknown tangential stresses  $\sigma_\theta$  and physical quantities at interior points need further investigation. In this paper, both boundary unknowns and physical quantities at interior points over different  $\delta$  are given.

Fig. 10 shows the tangential stress prediction  $\sigma_\theta$  at boundary node A (Note that the highest normalized eccentricity solved is  $\delta = 0.999999$ ). Fig. 11 shows the normalized radial stress  $\sigma_r$  at boundary node A, and the results obtained by using Ref. [Luo, Liu and Berger (1998)] and the FEM are also given to make comparison. In addition, for different angular coordinates, the radial and tangential stress pre-

Table 5: Radial and tangential stress prediction for  $\delta = 0.999999$ 

$\theta$	Stresses at boundary nodes		Stresses at interior points	
	$\sigma_r$	$\sigma_\theta$	$\sigma_r$	$\sigma_\theta$
0	-0.100000E+01	-0.250495E+00	-0.100000E+01	-0.250475E+00
$\pi/6$	-0.100000E+01	-0.250136E+00	-0.100498E+01	-0.254946E+00
$\pi/4$	-0.100000E+01	-0.250865E+00	-0.101078E+01	-0.261156E+00
$\pi/3$	-0.100000E+01	-0.252741E+00	-0.101807E+01	-0.271124E+00
$\pi/2$	-0.100000E+01	-0.261014E+00	-0.103417E+01	-0.301052E+00
$2\pi/3$	-0.100000E+01	-0.272464E+00	-0.104775E+01	-0.335890E+00
$5\pi/6$	-0.100000E+01	-0.281213E+00	-0.105608E+01	-0.362189E+00
$\pi$	-0.100000E+01	-0.284356E+00	-0.105881E+01	-0.371727E+00

diction for  $\delta = 0.999999$  at the boundary nodes  $(r_a, \theta)$  and at the interior points  $((r_a + r_b)/2, \theta)$  are given in Tab. 5.

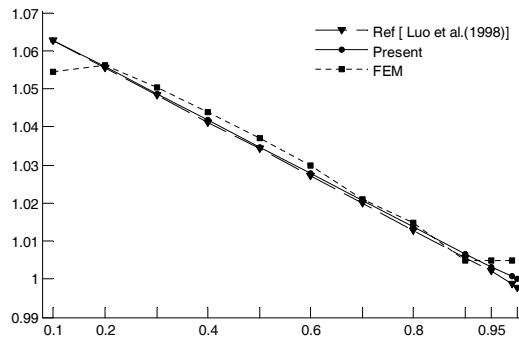


Figure 11: Radial stress prediction at the boundary node A.

## 6 Conclusions

In this paper, a new exact integration method for curvilinear geometries is presented and applied to deal with 2-D elastic problems of thin bodies. The conventional Gaussian quadrature can be replaced by the newly developed analytical integral formulas to deal with the nearly singular integrals. The strategy proposed in this paper adopted isoparametric quadratic elements to describe the integral kernel functions and the Jacobian. Owing to the employment of the parabolic arc, only a small number of elements need to be divided along the boundary, and high accuracy can be achieved without increasing more computational efforts. For thin-body

problems with thickness-to-length ratios ranging from 1E-1 to 1E-6, the stresses both on the boundary nodes and at interior points are all accurately calculated by using the presented strategy. In conclusion, the thin-body problem has been overcome successfully by using the proposed strategy, which indicates that the BEM is especially accurate and efficient for numerical analysis of thin body problems.

**Acknowledgement:** The research is supported by the National Natural Science Foundation of China (no. 10571110) and the Natural Science Foundation of Shandong Province of China (no. 2003ZX12).

## References

**Albuquerque, E.L.; Aliabadi, M.H.** (2008): A Boundary Element Formulation for Boundary Only Analysis of Thin Shallow Shells. *CMES: Computer Modeling in Engineering and Sciences*, vol. 29, no. 2, pp. 63-73.

**Atluri, S.N.** (2004a): *The meshless method (MLPG) for domain and BIE discretizations*. Forsyth, GA, USA, Tech Science Press.

**Atluri, S. N.** (2005): *Methods of computer modeling in engineering and the sciences*. Tech Science Press.

**Atluri, S.N.; Han, Z.D.; Rajendran, A.M.** (2004b): A new implementation of the meshless finite volume method through the MLPG “mixed” approach. *CMES: Computer Modeling in Engineering and Sciences*, vol. 6, no. 6, pp. 491-514.

**Atluri, S.N.; Han, Z.D.; Shen, P.S.** (2003): Meshless Local Petrov-Galerkin (MLPG) approaches for weakly-singular traction & displacement boundary integral equations. *CMES: Computer Modeling in Engineering & Sciences*, vol.4 (5)

**Atluri, S.N.; Liu, H.T.; Han, Z.D.** (2006): Meshless local Petrov-Galerkin (MLPG) mixed collocation method for elasticity problems. *CMES: Computer Modeling in Engineering and Sciences*, vol. 14, no. 3, pp. 141-152.

**Brebbia, C.A.; Tells, J.C.F.; Wrobel, L.C.** (1984): *Boundary Element Techniques*. Berlin, Heidelberg, New York, Tokyo: Springer.

**Chen, J.T.** (2000): Recent development of dual BEM in acoustic problems. *Comput Methods Appl Mech Eng*, vol. 188, pp. 833-845.

**Chen, J.T.; Chen, K.H.; Chen, C.T.** (2002): Adaptive boundary element method of time-harmonic exterior acoustics in two dimensions. *Comput Methods Appl Mech Eng*, vol. 191, pp. 3331–3345.

**Chen, X.L.; Liu, Y.J.** (2001): Thermal stress analysis of multi-layer thin films and coatings by an advanced boundary element method. *CMES: Computer Modeling in Engineering and Sciences*, vol. 2(3), pp. 337– 49.

- Davies, A.J.; Crann, D.; Kane, S.J.; Lai, C.H.** (2007): A Hybrid Laplace Transform/Finite Difference Boundary Element Method for Diffusion Problems. *CMES: Computer Modeling in Engineering and Sciences*, vol. 18, no. 2, pp. 79-85.
- Earlin, L.** (1992): Exact Gaussian quadrature methods for near-singular integrals in the boundary element method. *Eng Anal Bound Elem*, vol. 9, pp. 233-245.
- Fratantonio, M.; Rencis, J.J.** (2000): Exact boundary element integrations for two-dimensional Laplace equation. *Eng Anal Bound Elem*, vol. 24, pp. 325-42.
- Guiggiani, M.; Krishnasamy, G.; Rudolph, T.J.; Rizzo, F.J.** (1992): A general algorithm for the numerical solution of hypersingular BEM. *J Appl Mech*, vol. 59, pp. 604-627.
- Guz, A.N.; Menshykov, O.V.; Zozulya, V.V.; Guz, I.A.** (2007): Contact Problem for the Flat Elliptical Crack under Normally Incident Shear Wave. *CMES: Computer Modeling in Engineering and Sciences*, vol. 17, no. 3, pp. 205-214.
- Han, Z.D.; Atluri, S.N.** (2003): On simple formulations of weakly-singular traction & displacement BIE, and their solutions through Petrov-Galerkin approaches. *CMES: Computer Modeling in Engineering and Sciences*, vol. 4 (1), pp. 5-20.
- Han, Z.D.; Atluri, S.N.** (2007): A Systematic Approach for the Development of Weakly-Singular BIEs. *CMES: Computer Modeling in Engineering & Sciences*, vol. 21 (1), pp. 41-52.
- Jun, L.; Beer, G.; Meek** (1985): Efficient evaluation of integrals of order using Gauss quadrature. *Engng Anal*, vol. 2, pp. 118-23.
- Karlis, G.F.; Tsinopoulos, S.V.; Polyzos, D.; Beskos, D.E.** (2008): 2D and 3D Boundary Element analysis of Mode-I Cracks in Gradient Elasticity. *CMES: Computer Modeling in Engineering and Sciences*, vol. 26, no. 3, pp. 189-207.
- Li, J.; Wu, J.M.; Yu, D.H.** (2009): Generalized Extrapolation for Computation of Hypersingular Integrals in Boundary Element Methods. *CMES: Computer Modeling in Engineering and Sciences*, vol. 42, no. 2, pp. 151-175.
- Lifeng, M.A.; Alexander, M.; Korsunsky** (2004): A note on the Gauss-Jacobi quadrature formulae for singular integral equations of the second kind. *Int J Fract*, vol. 126, pp. 339-405.
- Liu, C.S.; Chang, C.W.; Chang, J.R.** (2008): A New Shooting Method for Solving Boundary Layer Equations in Fluid Mechanics. *CMES: Computer Modeling in Engineering and Sciences*, vol. 32, no. 1, pp. 1-15.
- Liu, Y.J.** (1998): Analysis of Shell-like Structures by the Boundary Element Method Based on 3-D Elasticity: Formulation and Verification. *Int J Numer Methods Eng*, vol. 41(3), pp.541-558.
- Luo, J.F.; Liu, Y.J.; Berger, E.J.** (1998): Analysis of two-dimensional thin struc-

tures (from micro- to nano-scales) using the boundary element method. *Comput Mech*, vol.22, pp. 404-412.

**Luo, J.F.; Liu, Y.J.; Berger, E.J.** (2000): Interfacial stress analysis for multi-coating systems using an advanced boundary element method. *Comput Mech*, vol. 24, pp. 448–55.

**Mukherjee, S.; Chati, M.K.; Shi, X.L.** (2000): Evaluation of nearly singular integrals in boundary element contour and node methods for three-dimensional linear elasticity. *Int J Sol Struct*, vol. 37, pp. 7633-7654.

**Niu, Z.R.; Cheng, C.Z.; Zhou, H.L.; Hu, Z.J.** (2007): Analytic formulations for calculating nearly singular integrals in two-dimensional BEM. *Eng Anal Bound Elem*, vol. 31, pp. 949–964.

**Okada, H.; Rajiyah, H.; Atluri, S.N.** (1989): A novel displacement gradient boundary element method for elastic stress analysis with high accuracy. *J. Applied Mechanics*, pp. 1-9.

**Okada, H.; Rajiyah, H.; Atluri, S.N.** (1989): Non-hyper-singular integral representations for velocity (displacement) gradients in elastic/plastic solids (small or finite deformations). *Computational Mechanics 4*, pp. 165-175.

**Okada, H.; Rajiyah, H.; Atluri, S.N.** (1990): A Full Tangent Stiffness Field-Boundary Element Formulation for Geometric and Material Nonlinear Problems of Solid Mechanics. *International Journal of Numerical Method in Engineering*, vol. 29, pp. 15-35.

**Padhi, G.S.; Sheno, R.A.; Moy, S.S.J.; McCarthy, M.A.** (2001): Analytical Integration of kernel shape function product integrals in the boundary element method. *Comput Struct*. Vol. 79, pp. 1325-1333.

**Sanz, J.A.; Solis, M.; Dominguez, J.** (2007): Hypersingular BEM for Piezoelectric Solids: Formulation and Applications for FractureMechanics. *CMES: Computer Modeling in Engineering and Sciences*, vol. 17, no. 3, pp. 215-229.

**Sladek, V.; Sladek, J.; Tanaka, M.** (1993): Nonsingular BEM formulations for thin-walled structures and elastostatic crack problems. *Acta Mechanica*, vol.99, pp. 173-190.

**Tanaka, M.; Matsumoto, T.; Nakamura, M.** (1991): *Boundary element method*. Baifukan Press, Tokyo (in Japanese).

**Tanaka, M.; Sladek, V.; Sladek, J.** (1994): Regularization techniques applied to BEM. *Appl Mech Rev*, vol. 47, pp. 457–499.

**Yoon, S.S.; Heister, S.D.** (2000): Analytic solution for fluxes at interior points for 2D Laplace equation. *Eng Anal Bound Elem*, vol. 24, pp. 155–60.

**Young, D.L.; Chen, K.H.; Chen, J.T.; Kao, J.H.** (2007): A Modified Method of

Fundamental Solutions with Source on the Boundary for Solving Laplace Equations with Circular and Arbitrary Domains. *CMES: Computer Modeling in Engineering and Sciences*, vol. 19, no. 3, pp. 197-221.

**Zhang, Y.M.; Gu, Y.; Chen, J.T.** (2009): Boundary layer effect in BEM with high order geometry elements using transformation. *CMES: Computer Modeling in Engineering & Sciences*, vol. 45, no. 3, pp. 227–247.

**Zhang, Y.M.; Wen, W.D.; Wang, L.M.; Zhao, X.Q.** (2004): A kind of new nonsingular boundary integral equations for elastic plane problems. *Acta Mech*, vol.36(3), pp. 311-321 (in Chinese).

**Zhang, Y.M.; Sun, C.L.** (2008): A general algorithm for the numerical evaluation of nearly singular boundary integrals in the equivalent non-singular BIES with indirect unknowns. *Journal of the Chinese Institute of Engineers*, vol. 31, pp. 437-447.

**Zhang, Y.M.; Sun, H.C.** (2000): Theoretic Analysis on Virtual Boundary Element. *Chinese J Comp Mech*, vol.17, pp. 56-62 (in Chinese).

**Zhang, Y.M.; Sun, H.C.** (2001): Analytical treatment of boundary integrals in direct boundary element analysis of plane potential and elasticity problems. *Appl Math Mech*, vol. 6, pp. 664-673.

**Zhang, X.S.; Zhang, X.X.** (2004): Exact integrations of two-dimensional high-order discontinuous boundary element of elastostatics problems. *Eng Anal Bound Elem*, vol. 28, pp. 725-732.

**Zhou, H. L.; Niu, Z.R.; Cheng, C.Z.; Guan, Z.W.** (2008): Analytical integral algorithm applied to boundary layer effect and thin body effect in BEM for anisotropic potential problems. *Comp and Struct*, vol.86, pp. 1656– 1671.